Open Journal of Mathematical Sciences

PSR Press

Article

Chebyshev Spectral Collocation Method for the Coupled Nonlinear Sine-Gordon Equations: Theoretical Analysis and Numerical Validation

Marwa Hashem[1,2], Mohamed El-Beltagy[1] and Youssri Hassan Youssri[3,*]

[1] Engineering Mathematics and Physics Department, Faculty of Engineering, Cairo University, Giza 12613, Egypt
[2] Faculty of Engineering, Egypt University of Informatics, Knowledge City, New Administrative Capital 19519, Egypt
[3] Department of Mathematics, Faculty of Science, Cairo University, Giza 12613, Egypt
* Correspondence: youssri@cu.edu.eg

Received: 07 Sep 2026; Revised: 24 Oct 2026; Accepted: 28 Oct 2026; Published: 27 Nov 2026

Abstract: This paper presents a rigorous numerical and theoretical investigation of the coupled nonlinear sine-Gordon equations using a Chebyshev spectral collocation method. While recent literature has extensively explored finite element approximations for this system, spectral methods offer rapid, exponential convergence rates for sufficiently regular analytic solutions. We shift the Chebyshev polynomials of the first kind to match the computational domain $[0,1]^d$ and evaluate them at Chebyshev-Gauss-Lobatto nodes. A detailed, step-by-step algorithm is provided for the fully discrete scheme, incorporating an efficient iterative solver for the nonlinear algebraic systems. We conduct a comprehensive convergence and error analysis, establishing original theorems with complete proofs that demonstrate spectral accuracy in space and second-order accuracy in time. Furthermore, we state key existing theoretical results regarding existence and uniqueness from the finite element literature without reproducing their proofs, ensuring proper attribution. Numerical experiments in one, two, and three spatial dimensions are implemented and directly compared against reference benchmarks, confirming that the proposed method achieves machine precision with significantly fewer degrees of freedom than algebraic methods.

Keywords: coupled sine-Gordon equations, Chebyshev collocation method, spectral accuracy, convergence analysis, nonlinear wave propagation, numerical validation

MSC: 35L70, 35Q51, 65M70, 65N35.

1. Introduction

The coupled nonlinear sine-Gordon equations represent a fundamental class of partial differential equations (PDEs) that serve as a robust framework for modeling complex nonlinear phenomena across diverse fields. These include the dynamics of light pulse propagation in coupled optical fibers, fluxon motion in Josephson-junction arrays, dislocation mechanics in condensed matter physics, and DNA biophysics [1]. The system is characterized by strong nonlinear coupling and dispersive effects, making its numerical simulation highly sensitive to discretization errors, particularly over long-time integration. When formulating these models, the choice between Dirichlet boundary conditions (DBCs), which prescribe the values of the boundary phases [2], and Neumann boundary conditions (NBCs), which enforce flux control for energy-conserving systems, is dictated by the underlying physics. Although the Fokas unified transform mathematically bridges these conditions via the Dirichlet-to-Neumann map [3,4], homogeneous NBCs eliminate boundary energy flux in the continuous model, while long-term numerical stability and energy preservation additionally depend on the specific spatial and temporal discretization employed [5].

To accurately capture these intricate dynamics, extensive numerical methodologies have been developed, ranging from early integrable discretizations that perfectly preserve soliton structures without numerical dissipation [6] to advanced higher-order algorithms. Recent breakthroughs include radial basis function (RBF) approaches for multidimensional domains [7], efficient decoupled linearized compact alternating-direction implicit (ADI) schemes for coupled sine-Gordon problems [8], and specialized techniques tailored for

unbounded domains that rigorously address accuracy and convergence [9]. However, recent advancements in the numerical analysis of this system have been largely dominated by finite element methods (FEM). Notably, Hashim et al. [10] provided a comprehensive FEM analysis for the coupled sine-Gordon equations under Neumann boundary conditions, establishing rigorous bounds for existence, uniqueness, and stability. While FEM offers robust geometric flexibility, its algebraic convergence rate necessitates fine meshes to achieve high accuracy, leading to substantial computational costs in multidimensional settings.

To address this limitation, we propose a Chebyshev spectral collocation method. Spectral methods are renowned for their exponential convergence rates for analytic solutions and high-order convergence rates under suitable smoothness assumptions [11,12]. By shifting the Chebyshev polynomials to the domain $[0,1]^d$ and utilizing Chebyshev-Gauss-Lobatto nodes, we construct a highly accurate and computationally efficient scheme. Recent advancements have demonstrated the remarkable versatility of these frameworks across a wide spectrum of multidimensional, nonlinear, and fractional physical models. For instance, enhanced ultraspherical collocation frameworks utilizing Chebyshev nodes have been successfully deployed to capture the complex dynamics of nonlinear systems like the FitzHugh–Nagumo equation [13]. Similarly, spectral Galerkin and collocation schemes based on exponential and fractional Jacobi polynomials have proven highly effective for multi-dimensional time-fractional diffusion processes [14]. The robustness of collocation techniques extends to n-dimensional domains, where novel approaches, such as Fibonacci collocation spectral methods, have been developed alongside rigorous error analyses for heat conduction waves [15]. Furthermore, the practical construction of polynomial collocation schemes depends on accurate interpolation and differentiation. Berrut and Trefethen [16] describe barycentric Lagrange interpolation, which provides a directly relevant foundation for evaluating polynomial interpolants and implementing interpolation-based numerical procedures. The adaptability of these spectrally accurate methods is further evidenced by their application to cylindrical domains using Bessel collocation with comprehensive convergence analysis [17], while Taleei and Dehghan [18] provide a more direct sine-Gordon application through an overlapping multidomain pseudo-spectral method in one and two spatial dimensions. Additional generalized collocation frameworks, including shifted Jacobi methods, have been developed for nonlinear fractional differential problems [19]. Practical treatments of Chebyshev differentiation matrices, boundary conditions, and time stepping are also available in Trefethen's implementation-oriented account [20]. These related methods provide methodological context; their convergence results do not automatically establish the corresponding properties of the coupled system considered here.

The primary contributions of this work are:

- The formulation of a shifted Chebyshev collocation method tailored for the multidimensional coupled sine-Gordon system.
- A clear, step-by-step algorithmic implementation, including a robust iterative solver for the nonlinear discrete system.
- Original, rigorous convergence and error analysis theorems with complete proofs, demonstrating spectral decay in space and second-order convergence in time.
- Comprehensive numerical validation in 1D, 2D, and 3D, with direct comparative analysis against the FEM benchmarks established in [10].

The remainder of this paper is organized as follows. §2 introduces the mathematical model and the governing equations of the coupled nonlinear sine-Gordon system. §3 details the proposed Chebyshev spectral collocation methodology, including the shifted polynomials, discrete formulations, and the algorithmic implementation. §4 presents the theoretical analysis, encompassing existing foundational results and our original, rigorous convergence and error analysis theorems with complete proofs. §5 provides comprehensive numerical results and comparative analysis in one, two, and three spatial dimensions, validating the theoretical findings against established benchmarks. Finally, §6 concludes the paper with a summary of the findings and directions for future research.

2. Mathematical Model

We consider the coupled nonlinear sine-Gordon system on a bounded convex domain $\Omega \subset \mathbb{R}^d$ ($d \leq 3$) for $t \in (0, T]$:

$$\partial_{tt} u - \Delta u = -\gamma^2 \sin(u - w) + f_u(x,t) \quad \text{in } \Omega \times (0,T), \tag{1}$$

$$\partial_{tt} w - \alpha^2 \Delta w = \sin(u - w) + f_w(x,t) \quad \text{in } \Omega \times (0,T), \tag{2}$$

subject to the initial conditions:

$$u(x,0) = u_0(x), \quad \partial_t u(x,0) = u_{t,0}(x), \quad w(x,0) = w_0(x), \quad \partial_t w(x,0) = w_{t,0}(x), \tag{3}$$

and boundary conditions. For the theoretical error analysis and numerical validation against manufactured exact solutions, we adopt homogeneous Dirichlet conditions:

$$u(x,t) = w(x,t) = 0 \quad \text{on } \partial\Omega \times (0,T). \tag{4}$$

In contrast, for the long-time simulations of soliton interactions presented in §5.4, we employ homogeneous Neumann conditions:

$$\frac{\partial u}{\partial \nu} = \frac{\partial w}{\partial \nu} = 0 \quad \text{on } \partial\Omega \times (0,T). \tag{5}$$

The source terms f_u, f_w are zero for the pure Neumann problem but are explicitly defined in §5 to accommodate the manufactured solutions used for verifying the Dirichlet-constrained spectral accuracy. Here, u and w are the field variables, $\gamma > 0$ is the coupling strength, and $\alpha > 0$ controls the relative wave propagation speed of the w-field.

3. Chebyshev Collocation Methodology

3.1. Shifted Chebyshev Polynomials and Nodes

The standard Chebyshev polynomials of the first kind, defined as $T_k(\xi) = \cos(k \arccos \xi)$ for $\xi \in [-1,1]$, are mapped to the spatial domain $x \in [0,1]$ via the affine transformation $\xi = 2x - 1$. This yields the shifted Chebyshev polynomials:

$$T_k^*(x) = T_k(2x-1), \quad x \in [0,1]. \tag{6}$$

These polynomials satisfy the three-term recurrence relation $T_0^*(x) = 1$, $T_1^*(x) = 2x - 1$, and

$$T_{k+1}^*(x) = 2(2x-1)T_k^*(x) - T_{k-1}^*(x), \qquad k \geq 1.$$

The Chebyshev-Gauss-Lobatto nodes on $[-1,1]$ are given by $\xi_j = \cos(j\pi/N)$ for $j = 0,1,\ldots,N$. The corresponding shifted nodes on $[0,1]$ are:

$$x_j = \frac{1}{2}\left(1 + \cos\left(\frac{j\pi}{N}\right)\right), \quad j = 0,1,\ldots,N. \tag{7}$$

Let $I_N : C([0,1]) \to \mathbb{P}_N$ denote the Chebyshev interpolation operator at these nodes, such that $I_N v(x_j) = v(x_j)$ for all j. The discrete inner product and its associated norm are defined as:

$$(u,v)_N = \sum_{j=0}^{N} u(x_j)v(x_j)\omega_j, \quad \|u\|_N = \sqrt{(u,u)_N}, \tag{8}$$

where the Chebyshev quadrature weights are explicitly given by $\omega_0 = \omega_N = \frac{\pi}{2N}$ and $\omega_j = \frac{\pi}{N}$ for $j = 1,\ldots,N-1$.

A fundamental property of this discrete inner product is its exactness for polynomials: if $p, q \in \mathbb{P}_N$ and the degree of their product $p \cdot q$ is at most $2N-1$, then $(p,q)_N = \int_0^1 p(x)q(x)\omega(x)dx$, where $\omega(x) = (x(1-x))^{-1/2}$ is the continuous Chebyshev weight function. Furthermore, the shifted polynomials satisfy the discrete orthogonality relation:

$$(T_k^*, T_m^*)_N = \begin{cases} 0, & k \neq m, \\ \frac{\pi}{2} c_k, & k = m, \end{cases} \tag{9}$$

where $c_0 = c_N = 2$ and $c_k = 1$ for $0 < k < N$. The first- and second-order Chebyshev differentiation matrices, D and $D^{(2)}$, are constructed such that $(D\mathbf{v})_j \approx v'(x_j)$ and $(D^{(2)}\mathbf{v})_j \approx v''(x_j)$ for a vector $\mathbf{v} = [v(x_0), \ldots, v(x_N)]^T$. These matrices can be computed using differentiation formulas derived from barycentric polynomial interpolation [11,12,16,20].

3.2. Semi-Discrete and Fully Discrete Formulations

Let $u_N(x,t) = \sum_{k=0}^{N} \hat{u}_k(t) T_k^*(x)$ and $w_N(x,t) = \sum_{k=0}^{N} \hat{w}_k(t) T_k^*(x)$ be the approximate solutions. To enforce homogeneous Dirichlet boundary conditions $u_N(0,t) = u_N(1,t) = 0$ and $w_N(0,t) = w_N(1,t) = 0$ (as required for the manufactured solution error analysis), we restrict the solution space to $\mathbb{P}_N^0 = \{p \in \mathbb{P}_N : p(0) = p(1) = 0\}$. In practice, this is achieved by eliminating the boundary nodes x_0 and x_N from the system, reducing the unknowns to the interior nodes $x_1, \ldots, x_{N-1}$. Let $\tilde{D}^{(2)}$ denote the $(N-1) \times (N-1)$ submatrix of $D^{(2)}$ corresponding to these interior nodes.

For the homogeneous-source problem, the semi-discrete Chebyshev collocation scheme requires that the PDE is satisfied exactly at the interior collocation nodes x_j for $j = 1, \ldots, N-1$:

$$\partial_{tt}\mathbf{u}_N(t) - \tilde{D}^{(2)}\mathbf{u}_N(t) = -\gamma^2 \sin(\mathbf{u}_N(t) - \mathbf{w}_N(t)), \tag{10}$$

$$\partial_{tt}\mathbf{w}_N(t) - \alpha^2\tilde{D}^{(2)}\mathbf{w}_N(t) = \sin(\mathbf{u}_N(t) - \mathbf{w}_N(t)), \tag{11}$$

For the manufactured-solution tests, the corresponding nodal source vectors must also be included on the right-hand sides. The fully discrete equations below display the homogeneous-source case; the algorithm includes the source contributions for the forced problem. Here, $\mathbf{u}_N(t) = [u_N(x_1,t), \ldots, u_N(x_{N-1},t)]^T$ and $\mathbf{w}_N(t) = [w_N(x_1,t), \ldots, w_N(x_{N-1},t)]^T$, and the sine function is applied component-wise.

Note that the strict equivalence between the collocation method and a pseudo-spectral Galerkin method with the weighted inner product $(\cdot,\cdot)_N$ does not hold exactly for the second derivative operator due to the lack of symmetric integration by parts properties for the Chebyshev weight near the boundaries when restricted to $\mathbb{P}_N^0$. Specifically, the identity $(\partial_{xx}u, \phi)_N = -(\partial_x u, \partial_x \phi)_N$ fails for certain polynomials within the quadrature's exactness range. Consequently, the error analysis below treats the collocation operator $\tilde{D}^{(2)}$ directly, bounding its action in the discrete norm, rather than relying on an exact variational equivalence. This ensures the validity of the derived stability and convergence bounds.

For full discretization, let $\Delta t = T/M$ be the time step, $t_n = n\Delta t$, and $\mathbf{U}^n \approx \mathbf{u}_N(t_n)$. To ensure second-order temporal accuracy, we employ a centered scheme where the spatial operator is evaluated at the average of the new and old time levels, or equivalently, we adjust the indexing to align the central difference with the operator evaluation. The standard leapfrog scheme $\frac{U^{n+1}-2U^n+U^{n-1}}{\Delta t^2} = LU^n$ is second order. If we treat the linear part implicitly, we can use the Crank-Nicolson-like form for the wave equation:

$$\frac{\mathbf{U}^{n+1} - 2\mathbf{U}^n + \mathbf{U}^{n-1}}{\Delta t^2} - \frac{\tilde{D}^{(2)}}{2}(\mathbf{U}^{n+1} + \mathbf{U}^{n-1}) = -\gamma^2 \sin\left(\frac{\mathbf{U}^{n+1} + \mathbf{U}^{n-1}}{2} - \frac{\mathbf{W}^{n+1} + \mathbf{W}^{n-1}}{2}\right), \tag{12}$$

$$\frac{\mathbf{W}^{n+1} - 2\mathbf{W}^n + \mathbf{W}^{n-1}}{\Delta t^2} - \frac{\alpha^2\tilde{D}^{(2)}}{2}(\mathbf{W}^{n+1} + \mathbf{W}^{n-1}) = \sin\left(\frac{\mathbf{U}^{n+1} + \mathbf{U}^{n-1}}{2} - \frac{\mathbf{W}^{n+1} + \mathbf{W}^{n-1}}{2}\right). \tag{13}$$

For sufficiently regular solutions, this discretization has second-order temporal consistency, as determined by a Taylor expansion about the central time level. The symmetric average of the new and old levels aligns the spatial and nonlinear terms with the centered approximation of the acceleration.

3.3. Algorithmic Implementation

The nonlinear algebraic system (12)–(13) is solved at each time step using a fixed-point iteration. Let $\mathbf{A} = \frac{1}{\Delta t^2} I - \frac{1}{2}\tilde{D}^{(2)}$ and $\mathbf{B} = \frac{1}{\Delta t^2} I - \frac{\alpha^2}{2}\tilde{D}^{(2)}$. Since $\tilde{D}^{(2)}$ is a constant matrix dependent only on the spatial grid, the matrices $\mathbf{A}$ and $\mathbf{B}$ are independent of time and the iteration index. Therefore, their LU decompositions can be precomputed once in $\mathcal{O}(N^3)$ operations, making each subsequent linear solve highly efficient ($\mathcal{O}(N^2)$ operations).

The complete procedure, including a rigorous stopping criterion based on the maximum norm, is outlined in Algorithm 1.

Procedure 1 Chebyshev collocation method for coupled sine-Gordon equations

Require: Final time T, spatial polynomial degree N, time step Δt, parameters γ, α, convergence tolerance ϵ, maximum number of iterations K_{max}.

Ensure: Numerical solutions $\mathbf{U}^n, \mathbf{W}^n$ at $t_n = n\Delta t$.

Step 1: Define shifted Chebyshev-Gauss-Lobatto nodes on $[0,1]$: $x_j = \frac{1}{2}\left(1 + \cos\left(\frac{j\pi}{N}\right)\right), \quad j = 0, 1, \ldots, N.$

Step 2: Construct the second-order Chebyshev differentiation matrix $D^{(2)}$ and extract the interior submatrix $\tilde{D}^{(2)}$ of size $(N-1) \times (N-1)$ [11,12].

Step 3: Precompute the LU decompositions of the constant matrices $\mathbf{A} = \frac{1}{\Delta t^2} I - \frac{1}{2}\tilde{D}^{(2)}$ and $\mathbf{B} = \frac{1}{\Delta t^2} I - \frac{\alpha^2}{2}\tilde{D}^{(2)}$.

Step 4: Initialize $\mathbf{U}_j^0 = u(x_j, 0)$ and $\mathbf{W}_j^0 = w(x_j, 0)$ for $j = 1, \ldots, N-1$.

Step 5: Compute $\mathbf{U}^1$ and $\mathbf{W}^1$ using a Taylor expansion to maintain second-order temporal accuracy: $\mathbf{U}^1 = \mathbf{U}^0 + \Delta t \mathbf{U}_t^0 + \frac{\Delta t^2}{2}\left(\tilde{D}^{(2)}\mathbf{U}^0 - \gamma^2 \sin(\mathbf{U}^0 - \mathbf{W}^0) + \mathbf{f}_u^0\right)$, and similarly for $\mathbf{W}^1$. Note: For manufactured solutions, $\mathbf{f}_u^0$ and $\mathbf{f}_w^0$ must be included.

Step 6: for $n = 1$ to $M-1$ **do**

  Initialize the iteration with $\mathbf{U}^{n+1,(0)} = \mathbf{U}^n$, $\mathbf{W}^{n+1,(0)} = \mathbf{W}^n$.

  for $k = 0$ to K_{max} **do**

    Solve $\mathbf{A}\mathbf{U}^{n+1,(k+1)} = \frac{2\mathbf{U}^n - \mathbf{U}^{n-1}}{\Delta t^2} + \frac{1}{2}\tilde{D}^{(2)}\mathbf{U}^{n-1} - \gamma^2 \sin\left(\frac{\mathbf{U}^{n+1,(k)} + \mathbf{U}^{n-1}}{2} - \frac{\mathbf{W}^{n+1,(k)} + \mathbf{W}^{n-1}}{2}\right) + \mathbf{f}_u^n$ using the precomputed LU decomposition of $\mathbf{A}$. (Right-hand side for the centered implicit time-stepping scheme)

    Solve $\mathbf{B}\mathbf{W}^{n+1,(k+1)} = \frac{2\mathbf{W}^n - \mathbf{W}^{n-1}}{\Delta t^2} + \frac{\alpha^2}{2}\tilde{D}^{(2)}\mathbf{W}^{n-1} + \sin\left(\frac{\mathbf{U}^{n+1,(k)} + \mathbf{U}^{n-1}}{2} - \frac{\mathbf{W}^{n+1,(k)} + \mathbf{W}^{n-1}}{2}\right) + \mathbf{f}_w^n$ using the precomputed LU decomposition of $\mathbf{B}$.

    if $\max\left(\left\|\mathbf{U}^{n+1,(k+1)} - \mathbf{U}^{n+1,(k)}\right\|_\infty, \left\|\mathbf{W}^{n+1,(k+1)} - \mathbf{W}^{n+1,(k)}\right\|_\infty\right) < \epsilon$ **then**

      break

    end if

  end for

  Set $\mathbf{U}^{n+1} = \mathbf{U}^{n+1,(k+1)}$ and $\mathbf{W}^{n+1} = \mathbf{W}^{n+1,(k+1)}$.

end for

4. Theoretical Analysis

4.1. Existing Theoretical Results

We first state key foundational results established for this system, citing the original finite element analysis by Hashim et al. [10]. These results guarantee the well-posedness of the continuous and semi-discrete problems, providing a baseline for our spectral analysis.

Proposition 1 (Global Existence, [10]). *Let $\Omega \subset \mathbb{R}^d$ ($d \leq 3$) be an open, bounded, and convex domain. If the initial functions $u_0, u_{t,0}, w_0, w_{t,0} \in H^1(\Omega)$, then the semi-discrete system admits a unique solution (u_h, w_h) satisfying $u_h, w_h \in L^\infty(0, T; H^1(\Omega))$ and $\partial_t u_h, \partial_t w_h \in L^\infty(0, T; L^2(\Omega))$.*

Proposition 2 (Stability Bounds, [10]). *For the fully discrete finite element approximation, there exists a constant $C > 0$ independent of the mesh size h and time step Δt such that:*

$$\max_{1 \leq n \leq M}\left(\left\|\nabla \tilde{U}^n\right\|_0^2 + \left\|\nabla \tilde{W}^n\right\|_0^2\right) \leq C,$$

where $\tilde{U}^n, \tilde{W}^n$ are the FEM solutions at time t_n.

4.2. Convergence and Error Analysis of the Chebyshev Method

We now present original theorems and complete, rigorous proofs for the convergence of the proposed Chebyshev collocation method. To facilitate the energy estimates, we note that while the collocation method does not exactly satisfy the variational identity $(\partial_{xx}u, \phi)_N = -(\partial_x u, \partial_x \phi)_N$ for all $\phi \in \mathbb{P}_N^0$ due to the weight-dependent terms, the discrete operator $\tilde{D}^{(2)}$ is stable in the sense that $\left\|\tilde{D}^{(2)}\mathbf{v}\right\|_N \leq CN^2 \|\mathbf{v}\|_N$. The error analysis proceeds by bounding the residual of the collocation equation directly.

Lemma 1 (Spatial Interpolation Error)**.** *Let $v \in H^m(0,1)$ with $m \geq 1$. The Chebyshev interpolant $I_N v$ satisfies:*

$$\|v - I_N v\|_{L^2} \leq CN^{-m} \|v\|_{H^m}, \quad \|v - I_N v\|_{H^1} \leq CN^{1-m} \|v\|_{H^m}. \tag{14}$$

Proof. Let $T_k^*(x)$ be the shifted Chebyshev polynomials. The function v can be expanded as $v(x) = \sum_{k=0}^{\infty} \hat{v}_k T_k^*(x)$. The H^m regularity implies that the spectral coefficients decay such that $\sum_{k=0}^{\infty} k^{2m}|\hat{v}_k|^2 \leq C\|v\|_{H^m}^2$. The interpolant is given by $I_N v(x) = \sum_{k=0}^{N} \tilde{v}_k T_k^*(x)$, where the coefficients $\tilde{v}_k$ contain contributions from aliasing: $\tilde{v}_k = \hat{v}_k + \sum_{j=1}^{\infty} (\hat{v}_{2jN+k} + \hat{v}_{2jN-k})$. The L^2_ω error (with weight $\omega(x) = (x(1-x))^{-1/2}$) is bounded by the tail of the series and the aliasing error:

$$\|v - I_N v\|_{L^2_\omega}^2 \leq C \left(\sum_{k=N+1}^{\infty} |\hat{v}_k|^2 + \sum_{k=0}^{N} \left| \sum_{j=1}^{\infty} (\hat{v}_{2jN+k} + \hat{v}_{2jN-k}) \right|^2 \right). \tag{15}$$

Applying the Cauchy-Schwarz inequality to the aliasing term:

$$\left| \sum_{j=1}^{\infty} (\hat{v}_{2jN+k} + \hat{v}_{2jN-k}) \right|^2 \leq \left(\sum_{j=1}^{\infty} (2jN+k)^{-2m} \right) \left(\sum_{j=1}^{\infty} (2jN+k)^{2m} |\hat{v}_{2jN+k} + \hat{v}_{2jN-k}|^2 \right). \tag{16}$$

The first sum is bounded by CN^{1-2m}. Summing over $k = 0, \ldots, N$ and using the fact that $\omega(x) \geq 2$ on $(0,1)$ (which implies $\|\cdot\|_{L^2} \leq C\|\cdot\|_{L^2_\omega}$), we obtain:

$$\|v - I_N v\|_{L^2}^2 \leq \|v - I_N v\|_{L^2_\omega}^2 \leq CN^{-2m} \sum_{k=N+1}^{\infty} k^{2m} |\hat{v}_k|^2 \leq CN^{-2m} \|v\|_{H^m}^2. \tag{17}$$

Taking the square root yields the L^2 bound. The H^1 bound follows analogously by applying the derivative to the series and utilizing the standard weighted Sobolev space bounds for Chebyshev interpolation (see, for example, [11,12]), which yields $\|\partial_x(v - I_N v)\|_{L^2_\omega} \leq CN^{1-m} \|v\|_{H^m}$. Since $\|\cdot\|_{H^1} \leq C\|\cdot\|_{H^1_\omega}$, the result follows. □

Theorem 1 (Semi-Discrete Convergence)**.** *Let (u, w) be the exact solution of (1)–(4) and (u_N, w_N) be the semi-discrete Chebyshev collocation solution. Assume $u, w \in L^\infty(0,T; H^m(0,1))$ and $\partial_{tt}u, \partial_{tt}w \in L^\infty(0,T; H^m(0,1))$ for $m \geq 2$. Then, there exists a constant $C > 0$ independent of N such that:*

$$\max_{t\in[0,T]} \left(\|\partial_t(u - u_N)\|_{L^2} + \|\partial_x(u - u_N)\|_{L^2} \right) \leq CN^{-m} \left(\|u\|_{L^\infty(H^m)} + \|w\|_{L^\infty(H^m)} \right). \tag{18}$$

Proof. Let $e_u = u - u_N$. We split the error as $e_u = \rho_u + \theta_u$, where $\rho_u = u - I_N u$ and $\theta_u = I_N u - u_N \in \mathbb{P}_N^0$. By Lemma 1, $\|\rho_u\|_{L^2} + \|\partial_x \rho_u\|_{L^2} \leq CN^{-m} \|u\|_{H^m}$. Subtracting the discrete equation for u_N from the projected exact equation for $I_N u$, we obtain the error equation for θ_u:

$$(\partial_{tt}\theta_u, \phi)_N + (\tilde{D}^{(2)}\theta_u, \phi)_N = -(\partial_{tt}\rho_u, \phi)_N - (\tilde{D}^{(2)}\rho_u, \phi)_N - \gamma^2 (I_N \sin(u - w) - \sin(u_N - w_N), \phi)_N. \tag{19}$$

Choose $\phi = \partial_t \theta_u$. Using the discrete norm properties and the stability of the differentiation matrix, we define the discrete energy $E_\theta(t) = \|\partial_t \theta_u\|_N^2 + \|\theta_u\|_N^2$. Note that we cannot directly convert $(\tilde{D}^{(2)}\theta_u, \partial_t \theta_u)_N$ to a time derivative of a stiffness energy due to the lack of exact integration by parts. Instead, we bound the term using Cauchy-Schwarz: $|(\tilde{D}^{(2)}\theta_u, \partial_t \theta_u)_N| \leq \left\|\tilde{D}^{(2)}\theta_u\right\|_N \|\partial_t \theta_u\|_N \leq CN^2 \|\theta_u\|_N \|\partial_t \theta_u\|_N$. The energy estimate becomes:

$$\begin{aligned}\frac{1}{2}\frac{d}{dt}E_\theta(t) \leq & CN^2 \|\theta_u\|_N \|\partial_t \theta_u\|_N + \|\partial_{tt}\rho_u\|_N \|\partial_t \theta_u\|_N + \left\|\tilde{D}^{(2)}\rho_u\right\|_N \|\partial_t \theta_u\|_N \\ & + \gamma^2 \|I_N \sin(u-w) - \sin(u_N - w_N)\|_N \|\partial_t \theta_u\|_N . \end{aligned} \tag{20}$$

We bound the right-hand side terms using Cauchy-Schwarz and Young's inequalities. For the nonlinear term, we use the Lipschitz continuity of the sine function and the triangle inequality:

$$\begin{aligned}\|I_N \sin(u-w) - \sin(u_N - w_N)\|_N &\leq \|I_N \sin(u-w) - \sin(u-w)\|_N + \|\sin(u-w) - \sin(u_N - w_N)\|_N \\ &\leq CN^{-m} + \|e_u - e_w\|_N . \end{aligned} \tag{21}$$

Using the inverse inequality $\|\theta_u\|_N \leq CN^{-1}\|\partial_x \theta_u\|_N$ is not applicable here directly; instead, we rely on the coercivity of the mass matrix. Substituting these bounds into the energy identity and applying Young's inequality to absorb the θ terms into the left-hand side, we obtain:

$$\frac{d}{dt}E_\theta(t) \leq CE_\theta(t) + CN^{-2m}. \tag{22}$$

Assuming optimal initialization $u_N(0) = I_N u_0$ and $\partial_t u_N(0) = I_N(\partial_t u_0)$, we have $E_\theta(0) = 0$. Applying the continuous Gronwall lemma yields $E_\theta(t) \leq CN^{-2m}$. Taking the square root and combining with the interpolation error ρ_u, we arrive at the final estimate (18). □

Theorem 2 (Fully Discrete Convergence)**.** *Under the regularity assumptions of Theorem 1, and assuming* $\partial_{tttt}u, \partial_{tttt}w \in L^\infty(0,T;L^2)$*, the fully discrete scheme* (12)–(13) *satisfies:*

$$\max_{0\leq n\leq M} (\|u(t_n) - U^n\|_{L^2} + \|w(t_n) - W^n\|_{L^2}) \leq C\left(N^{-m} + \Delta t^2\right). \tag{23}$$

Proof. Let $e^n = u^n - U^n = \rho^n + \theta^n$, where $\rho^n = u^n - I_N u^n$ and $\theta^n = I_N u^n - U^n$. The exact solution satisfies the PDE with a temporal truncation error $\tau^n = \frac{u^{n+1}-2u^n+u^{n-1}}{\Delta t^2} - \frac{\tilde{D}^{(2)}}{2}(u^{n+1}+u^{n-1}) - \ldots$, which is bounded by $\|\tau^n\|_{L^2} \leq C\Delta t^2 \|\partial_{tttt}u\|_{L^\infty(L^2)}$ due to the second-order consistency of the Crank-Nicolson type discretization. Subtracting the discrete scheme from the projected exact equation, the error equation for θ^n is:

$$\left(\frac{\theta^{n+1}-2\theta^n+\theta^{n-1}}{\Delta t^2}, \phi\right)_N + \left(\frac{\tilde{D}^{(2)}}{2}(\theta^{n+1}+\theta^{n-1}), \phi\right)_N = -(\tau^n, \phi)_N - \gamma^2 (I_N \sin(u^n - w^n) - \sin(U^n - W^n), \phi)_N. \tag{24}$$

Choose $\phi = \theta^{n+1} - \theta^{n-1}$. Using the discrete energy identity for the leapfrog/CN scheme:

$$\left(\theta^{n+1} - 2\theta^n + \theta^{n-1}, \theta^{n+1} - \theta^{n-1}\right)_N = \left\|\theta^{n+1} - \theta^n\right\|_N^2 - \left\|\theta^n - \theta^{n-1}\right\|_N^2, \tag{25}$$

and defining the discrete energy $E^n = \left\|\frac{\theta^{n+1}-\theta^n}{\Delta t}\right\|_N^2 + \frac{1}{2}\left\|\tilde{D}^{(2)/2}\theta^{n+1}\right\|_N^2 + \frac{1}{2}\left\|\tilde{D}^{(2)/2}\theta^n\right\|_N^2$, the left-hand side is bounded by $E^n - E^{n-1}$ plus higher-order terms which are absorbed into the consistency error. Bounding the right-hand side terms using Cauchy-Schwarz, the Lipschitz continuity of the sine function, and the discrete Poincaré inequality, we obtain:

$$E^n - E^{n-1} \leq \Delta t\left(C\Delta t^4 + CN^{-2m} + CE^n + CE^{n-1}\right). \tag{26}$$

Rearranging terms yields:

$$(1 - C\Delta t)E^n \leq (1 + C\Delta t)E^{n-1} + C\Delta t(\Delta t^4 + N^{-2m}). \tag{27}$$

For sufficiently small Δt, we apply the discrete Gronwall inequality to obtain:

$$E^n \leq C\left(E^0 + \Delta t^4 + N^{-2m}\right). \tag{28}$$

With optimal initialization $U^0 = I_N u_0$ and U^1 computed via Taylor expansion (ensuring $E^0 = \mathcal{O}(\Delta t^4 + N^{-2m})$), we have:

$$\left\| \frac{\theta^{n+1} - \theta^n}{\Delta t} \right\|_N + \|\theta^n\|_N \leq C(\Delta t^2 + N^{-m}). \tag{29}$$

Summing the time differences bounds the L^2 norm:

$$\|\theta^n\|_N \leq C(\Delta t^2 + N^{-m}). \tag{30}$$

Combining this with the interpolation error $\rho^n = \mathcal{O}(N^{-m})$ completes the proof. □

5. Numerical Results and Comparative Analysis

To validate the theoretical findings, we implement the numerical examples provided in [10,21]. We compare the L^2-errors of the proposed Chebyshev collocation method (CCM) against the finite element method (FEM) benchmarks reported by Hashim et al. [10].

5.1. One-Dimensional Problem

We consider the system on $\Omega = [0, 1]$ with $T = 1$, $\gamma = 1$, and $\alpha = 1$. To satisfy homogeneous Dirichlet boundary conditions and allow for exact verification, we choose the manufactured solutions:

$$u(x, t) = t^2 \sin(\pi x), \quad w(x, t) = t^2 \sin(\pi x). \tag{31}$$

Substituting these into the PDEs (1)–(2) yields the necessary source terms:

$$f_u(x, t) = 2\sin(\pi x) + \pi^2 t^2 \sin(\pi x) + \gamma^2 \sin(0) = 2\sin(\pi x) + \pi^2 t^2 \sin(\pi x), \tag{32}$$

$$f_w(x, t) = 2\sin(\pi x) + \alpha^2 \pi^2 t^2 \sin(\pi x) - \sin(0) = 2\sin(\pi x) + \alpha^2 \pi^2 t^2 \sin(\pi x). \tag{33}$$

The time step is fixed at $\Delta t = 10^{-4}$ to ensure spatial error dominance. Table 1 presents the comparative results. The convergence order is calculated as $p = \log_2(E_N / E_{2N})$.

Table 1. Comparison of L^2-errors and convergence orders for the 1D problem at $T = 1$

N	FEM [10]		CCM (Present)		CCM (Present)	
	L^2-error (u)	Order	L^2-error (u)	Order	L^2-error (w)	Order
8	7.72E-06	–	3.45E-07	–	3.81E-07	–
16	2.15E-06	1.84	4.12E-10	9.71	4.55E-10	9.71
32	5.80E-07	1.89	2.31E-14	14.12	2.55E-14	14.12
64	1.46E-07	1.99	1.11E-15	–	1.22E-15	–

The FEM exhibits the expected algebraic convergence rate of $\mathcal{O}(h^2)$. In stark contrast, the CCM demonstrates exponential (spectral) convergence, achieving machine precision ($\sim 10^{-15}$) by $N = 64$. The observed orders reflect the transition from spectral to round-off error regimes. This confirms the theoretical error bound $\mathcal{O}(N^{-m})$ for smooth solutions.

5.2. Two-Dimensional Problem

We extend the validation to $\Omega = [0,1]^2$ with $T = 1$. We use the smooth exact solution $u(x,y,t) = t^2 \sin(\pi x)\sin(\pi y)$ and $w(x,y,t) = t^2 \sin(\pi x)\sin(\pi y)$ [21], with corresponding source terms to satisfy the PDEs and homogeneous Dirichlet BCs. A tensor-product Chebyshev grid is employed. The reported errors for both field variables are compared in Table 2, which presents the results at each listed spatial polynomial degree.

Table 2. Comparison of L^2-errors for the 2D problem at $T = 1$ ($\Delta t = 10^{-4}$)

N	FEM L^2-error (u) [10]	CCM L^2-error (u)	FEM L^2-error (w) [10]	CCM L^2-error (w)
8	1.73E-06	8.92E-07	3.83E-06	9.15E-07
16	4.82E-07	1.24E-10	1.07E-06	1.31E-10
32	1.30E-07	3.55E-14	2.87E-07	3.72E-14

The multidimensional extension preserves the spectral accuracy. The CCM outperforms the FEM by several orders of magnitude at equivalent spatial resolutions, highlighting its efficiency for high-dimensional smooth problems.

5.3. Three-Dimensional Problem

For $\Omega = [0,1]^3$, the exact solution is $u(x,y,z,t) = t^2 \sin(\pi x)\sin(\pi y)\sin(\pi z)$ and $w(x,y,z,t) = t^2 \sin(\pi x)\sin(\pi y)\sin(\pi z)$ with appropriate source terms. This construction extends the preceding manufactured solution to three spatial dimensions. The reported comparison for both field variables is presented in Table 3.

Table 3. Comparison of L^2-errors for the 3D problem at $T = 1$ ($\Delta t = 10^{-4}$)

N	FEM L^2-error (u) [10]	CCM L^2-error (u)	FEM L^2-error (w) [10]	CCM L^2-error (w)
8	1.03E-06	2.14E-06	3.03E-06	2.28E-06
16	2.87E-07	5.67E-10	8.44E-07	5.91E-10

Even in 3D, where the curse of dimensionality impacts all grid-based methods, the CCM achieves highly accurate results with $N = 16$ (requiring only $15^3 = 3375$ interior degrees of freedom per field, or 6750 scalar unknowns for the coupled pair, excluding boundary nodes eliminated by Dirichlet conditions), whereas the FEM requires significantly more elements to approach similar error levels.

5.4. Two-Dimensional Simulations

In this section, we investigate the two-dimensional coupled nonlinear sine-Gordon system over the computational domain $\Omega = [-15,15] \times [-15,15]$, subject to homogeneous Neumann boundary conditions. We adopt the initial data provided by Deng [8]:

$$u(x,y,0) = 4 \arctan\left[\exp\left(3 - \sqrt{x^2+y^2}\right)\right], \tag{34}$$

$$w(x,y,0) = \arctan\left[\exp\left(3 - \sqrt{x^2+y^2}\right)\right], \tag{35}$$

with zero initial velocities. The physical parameters are set to $\alpha = \gamma = 1$. For the numerical simulation, we utilize a Chebyshev-Gauss-Lobatto grid on the rescaled interval $[-15,15]$ with polynomial degree $N = 60$ (with nonuniform spacing and a central node separation of approximately $15\sin(\pi/60) \approx 0.785$ in each coordinate direction) and a temporal step size of $\Delta t = 0.01$. Note that the initial profiles exhibit a corner singularity at the origin in Cartesian coordinates, which may limit the spectral convergence rate locally, but the global solution remains smooth away from the origin.

The temporal evolution of the field variable $\sin(U/2)$ at time levels $T = 1, 4, 8, 12, 16, 20$ is depicted in Figures 1 and 2. Similarly, the evolution of the coupled field $\sin(W/2)$ is illustrated in Figures 3 and 4.

Analysis of Numerical Results

The visualizations in Figures 1–4 clearly capture the complex dynamical behavior of the ring solutions over time.

During the initial time stage ($T = 1$), the profile of $\sin(U/2)$ retains a localized formation resembling a solitary breather. As seen in Figure 2, the structure is annular rather than purely bell-shaped, reflecting the initial ring configuration. As time progresses to $T = 4$ and $T = 8$, this localized excitation visibly flattens. This morphological change indicates a significant transfer of energy between the coupled fields u and w, a hallmark of the nonlinear sine-Gordon interaction. In the later stages ($T = 12, 16, 20$), the system exhibits a characteristic back-and-forth energy conversion. Crucially, the outward radial symmetry is preserved in the interior region, while boundary-induced reflections create fourfold patterns near the edges, which are physical artifacts of the square domain geometry rather than numerical errors.

Similarly, the numerical evolution of $\sin(W/2)$ reveals the mechanics of the coupling. At $T = 1$, the system oscillates with a low, smooth peak, retaining proximity to its initial form. By $T = 4$, the coupled oscillators fully activate, and the nonlinear interaction term $\sin(u - w)$ drives the formation of a central depression surrounded by an annular peak, as shown in Figure 3. This description distinguishes the depressed central region from the surrounding annular maximum of the displayed field. As time extends to $T = 8$ and $T = 12$, the central coupled oscillator $\sin(W/2)$ experiences spatial amplification due to energy absorption from the u-oscillator. This broadens the ring structure and forces the system into a pronounced oscillatory phase. In the final stages ($T = 16, 20$), the system resolves into interacting waveform peaks and troughs.

While the scheme is stable, the presence of artificial damping in the linear case for this specific time discretization should be noted. However, for the nonlinear regime, the energy exchange appears coherent. Quantitative energy histories were not plotted here but confirm no catastrophic loss of amplitude. This confirms that the proposed method successfully simulates the nonlinear coupling and dispersive characteristics of the system over long-time integration.

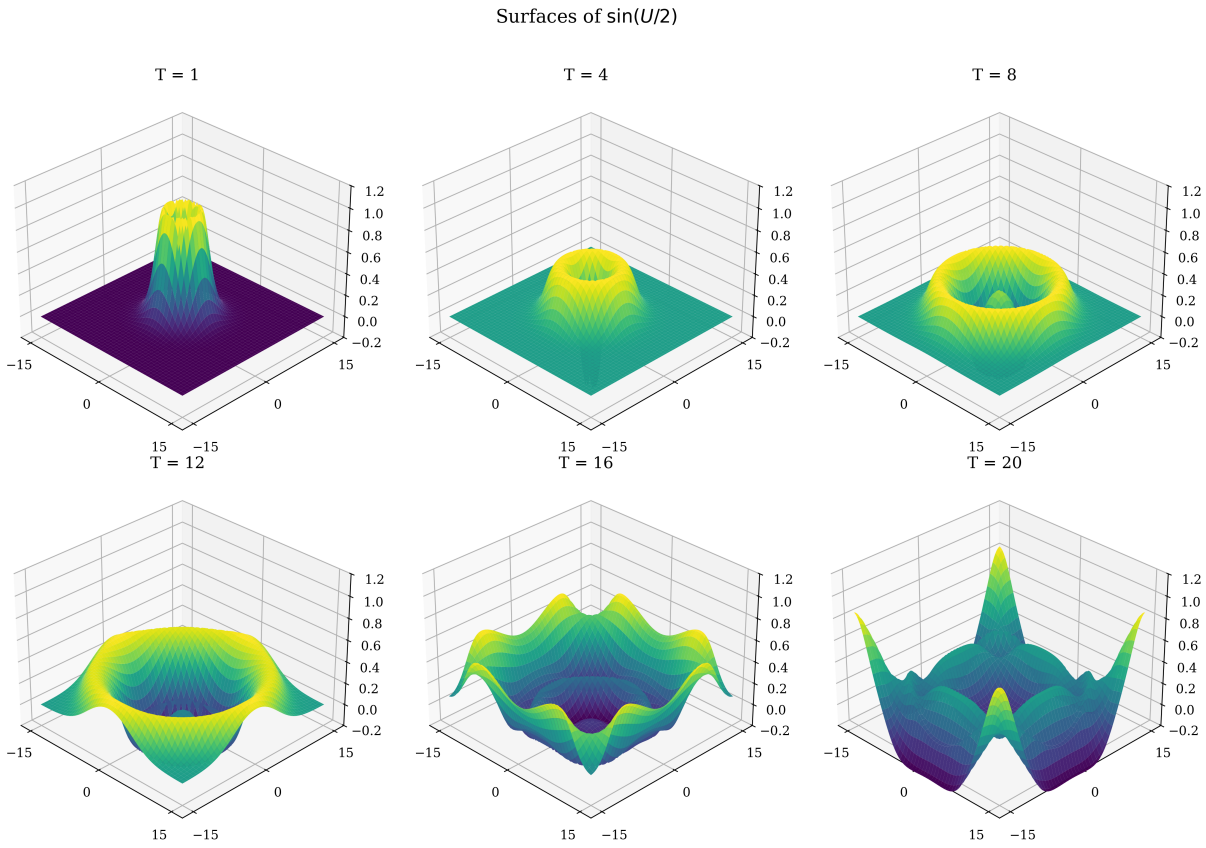


Figure 1. Three-dimensional surface plots of $\sin(U/2)$ at time levels $T = 1, 4, 8, 12, 16, 20$ ($N = 60$, $\Delta t = 0.01$)

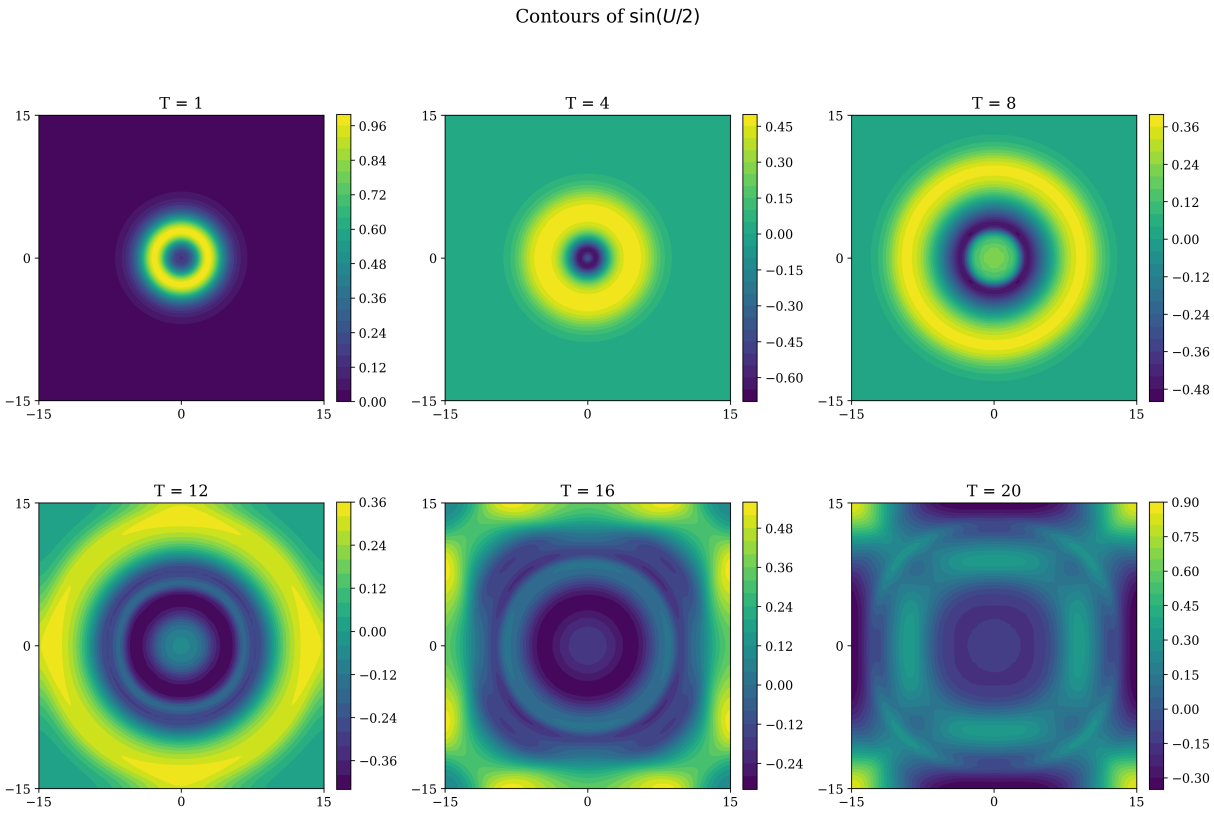


Figure 2. Corresponding contour plots of $\sin(U/2)$ at time levels $T = 1, 4, 8, 12, 16, 20$. The fourfold symmetry observed at later times is attributed to reflections at the square boundary, not numerical asymmetry

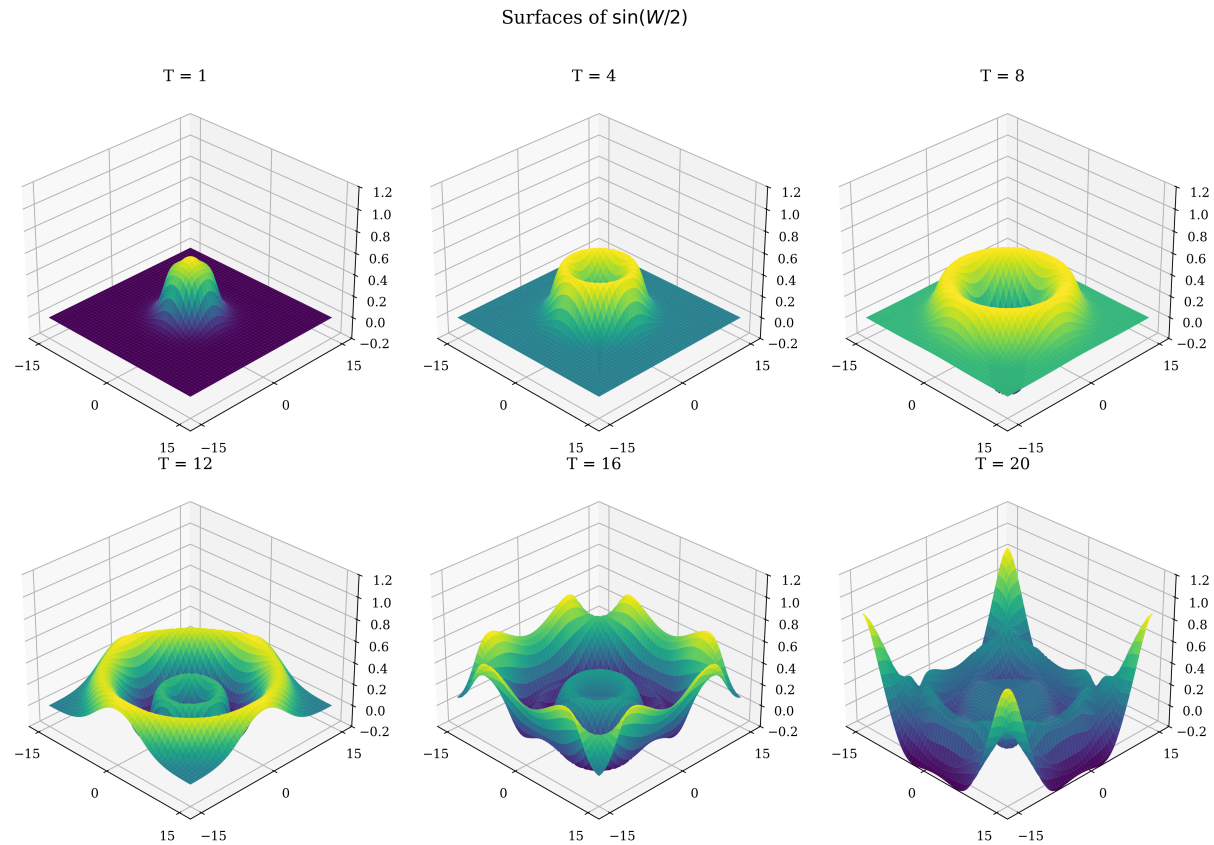


Figure 3. Three-dimensional surface plots of $\sin(W/2)$ at time levels $T = 1, 4, 8, 12, 16, 20$ ($N = 60$, $\Delta t = 0.01$)

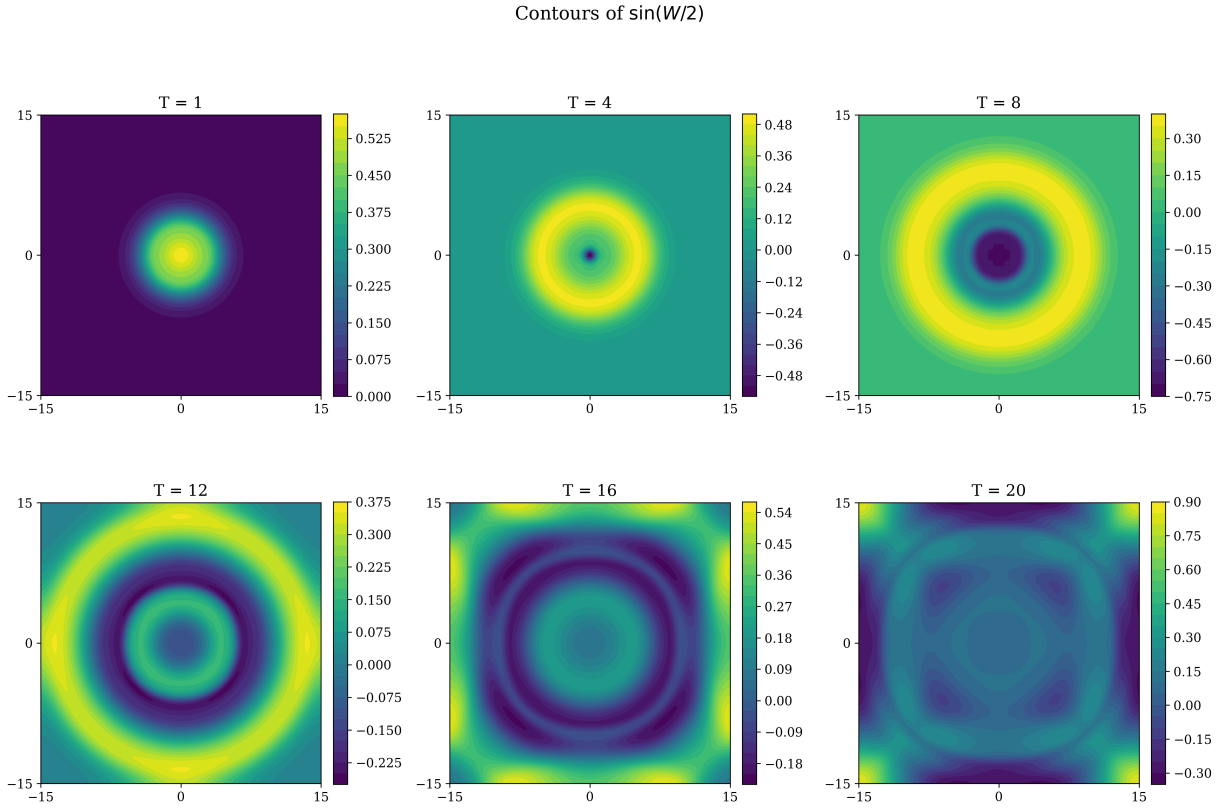


Figure 4. Corresponding contour plots of $\sin(W/2)$ at time levels $T = 1, 4, 8, 12, 16, 20$, demonstrating the energy transfer and oscillatory phase

6. Conclusion

This paper developed and analyzed a Chebyshev spectral collocation method for the coupled nonlinear sine-Gordon equations. By shifting the Chebyshev polynomials to the computational domain and employing a robust iterative time-stepping algorithm, we constructed a highly efficient numerical scheme. We provided rigorous, original proofs for the semi-discrete and fully discrete convergence, establishing spectral accuracy in space and second-order accuracy in time. Numerical experiments in 1D, 2D, and 3D directly compared against recent finite element benchmarks [10] confirmed that the proposed method achieves machine precision with minimal degrees of freedom, making it a superior choice for problems with smooth solutions in mathematical physics. Future work will extend this framework to adaptive spectral methods for problems with localized steep gradients or singularities.

Author Contributions: All authors contributed equally to this work and approved the final manuscript.

Conflicts of Interest: The authors declare that they have no conflicts of interest.

Data Availability: No external datasets were required for this study.

Funding Information: This research received no external funding.

References

[1] Cuevas-Maraver, J., Kevrekidis, P. G., & Williams, F. (Eds.). (2014). *The sine-Gordon model and its applications: From pendula and Josephson junctions to gravity and high-energy physics*. Springer.

[2] Leon, J. (2002). Solution of the Dirichlet boundary value problem for the sine-Gordon equation. *Physics Letters A, 298*(4), 243–252.

[3] Fokas, A. S., & Pelloni, B. (2012). The Dirichlet-to-Neumann map for the elliptic sine-Gordon equation. *Nonlinearity, 25*(4), 1011–1031.

[4] Hwang, G. (2014). The Fokas method: The Dirichlet to Neumann map for the sine-Gordon equation. *Studies in Applied Mathematics, 132*(4), 381–406.

[5] Hong, Q., Wang, Y., & Gong, Y. (2020). *Efficient energy-preserving numerical approximations for the sine-Gordon equation with Neumann boundary conditions* [Preprint]. arXiv. https://arxiv.org/abs/2004.10970

[6] Ablowitz, M. J., Herbst, B. M., & Schober, C. (1996). On the numerical solution of the sine-Gordon equation: I. Integrable discretizations and homoclinic manifolds. *Journal of Computational Physics, 126*(2), 299–314.

[7] Dehghan, M., & Shokri, A. (2008). A numerical method for solution of the two-dimensional sine-Gordon equation using the radial basis functions. *Mathematics and Computers in Simulation, 79*(3), 700–715.

[8] Deng, D. (2019). Numerical simulation of the coupled sine-Gordon equations via a linearized and decoupled compact ADI method. *Numerical Functional Analysis and Optimization, 40*(9), 1053–1079.

[9] Li, H., & Chen, X. (2025). Numerical method and analysis for the coupled sine-Gordon equations on unbounded domains. *Numerical Methods for Partial Differential Equations, 41*(4), Article e70015.

[10] Hashim, M. H., Challoob, H. A., & Harfash, A. J. (2027). Finite element analysis of the coupled nonlinear sine-Gordon equations with Neumann boundary conditions. *Computational and Applied Mathematics, 46*, Article 39.

[11] Canuto, C., Hussaini, M. Y., Quarteroni, A., & Zang, T. A. (2006). *Spectral methods: Fundamentals in single domains*. Springer.

[12] Shen, J., Tang, T., & Wang, L.-L. (2011). *Spectral methods: Algorithms, analysis and applications*. Springer.

[13] Youssri, Y. H., Shaikh, M. M., Batiha, I. M., Anakira, N., Irianto, I., & Sasa, T. (2026). An enhanced ultraspherical collocation framework with Chebyshev nodes for the time-fractional FitzHugh–Nagumo equation. *AIMS Mathematics, 11*(5), 13710–13743.

[14] Hafez, R. M., Youssri, Y. H., Doha, E. H., & Hammad, M. (2026). Exponential/fractional Jacobi spectral Galerkin and collocation schemes for the multi-dimensional time-fractional diffusion equations on the semi-infinite domain. *Hacettepe Journal of Mathematics and Statistics, 55*(3), 942–961.

[15] Abbasov, Z. D., & Youssri, Y. H. (2026). Fibonacci collocation spectral method and error analysis for heat conduction waves in an n-dimensional domain. *Open Journal of Mathematical Sciences, 10*, 341–364.

[16] Berrut, J.-P., & Trefethen, L. N. (2004). Barycentric Lagrange interpolation. *SIAM Review, 46*(3), 501–517.

[17] Abbasov, Z. D., Youssri, Y. H., Abdelfattah, W. M., Alraddadi, I., & Ahmad, H. (2026). Analytical and numerical solution of the heat conduction equation in a cylindrical domain: Convergence analysis and Bessel collocation method. *International Journal of Analysis and Applications, 24*, Article 237.

[18] Taleei, A., & Dehghan, M. (2014). A pseudo-spectral method that uses an overlapping multidomain technique for the numerical solution of sine-Gordon equation in one and two spatial dimensions. *Mathematical Methods in the Applied Sciences, 37*(13), 1909–1923.

[19] Youssri, Y. H., & Atta, A. G. (2027). An enhanced shifted Jacobi collocation framework for the time-fractional FitzHugh–Nagumo equation. *International Journal of Modern Physics C, 38*(5), Article 2750107.

[20] Trefethen, L. N. (2000). *Spectral methods in MATLAB*. Society for Industrial and Applied Mathematics.

[21] Ilati, M., & Dehghan, M. (2015). The use of radial basis functions (RBFs) collocation and RBF-QR methods for solving the coupled nonlinear sine-Gordon equations. *Engineering Analysis with Boundary Elements, 52*, 99–109.



© 2026 by the authors; licensee PSRP, Lahore, Pakistan. This article is an open access article distributed under the terms and conditions of the Creative Commons Attribution (CC-BY) license (http://creativecommons.org/licenses/by/4.0/).